Validation THUMSv4.1 head model in Visual Performance Solution and development of model-specific head injury criteria: skull fracture, mild Diffuse Axonal injury and subdural haematoma

Debasis Sahoo, Dhaval Jani, Giacomo Marini

Abstract The objective of this study was to validate the head model of THUMSv4.1 in Virtual Performance Solution occupant model and to develop model-specific head injury criteria: skull fracture, mild Diffuse Axonal injury (mDAI) and subdural haematoma (SDH). Mesh and materials were updated to improve the biofidelity response and the stability of the original model. The updated head model was then used to replicate different types of head trauma: skull fracture (N = 91), mDAI (78) and SDH (80). Survival analysis was used to develop model-specific injury risk functions. A comparative study with currently available kinematic criteria was performed for the relevant injury mechanism (e.g. for mDAI: DAMAGE, HIC, CIBIC). The improved head model is in good agreement with experimental data regarding skull, brain and bridging veins response. The proposed skull fracture injury risk is based on internal energy at element level. mDAI risk function is based on a combined strain and strain rate metric named brain injury score (BIS). Strain of bridging veins was used for assessing SDH injury risk. The comparison with real accident scenarios showed a good prediction capability. This study emphasises the use of tissue level parameter to predict head injury.

Keywords Brain strain, brain strain rate, Finite element head modeling, head trauma simulation, injury tolerance limit.

I. INTRODUCTION

Traumatic brain injury (TBI) prevails as the leading cause of disability and death in spite of abundant research and regulations [1-2]. Around 2.5 million severe health-related issues are associated with TBI in the USA [3]. In Europe, TBI incident rate ranges from 47.3 to 694 per 100,000 population annually [4]. The primary source of TBI includes falls, motor-vehicle crashes, pedestrian accidents, sports injuries and military accidents. However, motor-vehicle crashes contribute the highest percentage of TBI-related fatalities [5]. TBI ranges from mild (having concussion with brief loss of consciousness) to severe (an extended period of unconsciousness or memory loss after the injury). According to Abbreviated injury scale (AIS) code definition (code: 161002.2 or 161006.3) the injuries sustained by mild TBI patients can be between AIS2-3 [6].

Over the recent decades several Finite Element (FE) head models have been developed to investigate the head injury mechanism [8-11]. Most of the head models implement a hyper viscoelastic material model for the brain [8][9-12], except for a few models that use a linear viscoelastic material model [7][9]. Due to the differences in material implementation, modeling and FE software platform, the comparison of the predicted brain behaviour could result in significant challenges [13].

Several methods have been proposed to assess brain injury probability based on different metrics. Prior to the advent of state-of-the-art FE human body models (HBMs), injury criteria were mainly based on head kinematics. These presented limitations, however, especially in the case of blunt-like trauma or blast-induced head injury, where the lack of head acceleration measurement hinders the use of kinematics-based injury criteria. Furthermore, though experiments with post-mortem human subjects (PMHS) provide valuable information, their application is limited due to their inability to accurately depict the responses of a living human. The use of anthropometric test devices (ATDs, i.e. dummies) also has limitations, since the physical measurements are limited to a few locations as too many sensors may affect the physics of the system [14]. HBMs, on the other hand, have the ability to simulate complex loading scenarios and have flexibility in generating the desired

D. Sahoo (e-mail: debasis.sahoo@volkswagen.de; tel: +49 15229200124) is a safety engineer at VW, Wolfsburg, Germany; the present study was conducted when employed at VAIVA, Gaimersheim, Germany. D. Jani is a safety engineer at VAIVA, Gaimersheim, Germany. G. Marini is a safety engineer at Audi, Ingolstadt, Germany.

numerical data, which can facilitate a comprehensive understanding of injury mechanism.

Instead of using head accelerations for brain injury evaluation, the ability to describe brain tissue-level response is a key factor in understanding the injury mechanism [14]. Based on FE head models and head trauma simulations, brain pressure, Von-Mises stress and brain strain are the most common parameters used to predict brain injury [9][15-16]. Recent studies reported the use of maximum principal strain for injury prediction in 335 reconstructed cases [17]. However, this method predicted severe TBI in 14 non-injured volunteer experiments cases [17]. In the current study AIS 2+ injury level is considered as in most of the vehicle and sport accidents, a concussion with brief loss of consciousness is the most diagnosed injury as reported in accident databases [18-19] and literatures [20-22].

Models of biological systems and structures require an extended validation on both material and organ level. In particular, biological material such as brain tissue exhibits time-dependent response to mechanical loads, which could eventually influence the failure characteristic of the material [23]. The bulk modulus of the brain tissue is roughly five to six orders of magnitude larger than the shear modulus [24]. Hence it is likely that, for a given impact, the isochoric deformation of the brain tissue is predominant. A rapid elongation of the axon was shown as a leading cause of Diffuse Axonal Injury (DAI) [25]. Based on statistical analysis, both the strain rate and the axonal elongation presented a high correlation with the occurrence of AIS2+ brain injuries in 125 accident reconstructions [26]. The combination of strain and strain rate therefore should be considered for the development of a realistic brain injury criterion as described in [27].

The aim of this study was to validate the head model of the 50th percentile male THUMS 4.1 (Visual Performance Solution (VPS), ESI group) occupant model and to develop tissue-based injury criteria for AIS2+ brain injury, Subdural Haematoma injury and skull fracture. The injury criteria were then verified using a dataset of real accident reconstructions that was available at Audi.

II. METHODS

The head model of the THUMSv4.1 AM50 was used as the basis for the current study. All simulations were performed in VPS Version 2022.04. The skull FE model comprises parietal, occipital, frontal, temporal, ethnoid, sphenoid, nasal, vomer, lacrimal, palatine, maxilla, zygomatic and mandible bones. All the skull bones have cortical bone modeled with shell elements and inner spongy bone with mostly one layer of solid elements, as shown in Fig. 1. The sutures are modeled with solid elements and function as a connection between different cranial bones. The brain model consists of cerebrum, cerebellum, brainstem with distinct white and gray matter, cerebral spinal fluid (CSF) and sagittal sinus modeled with solid elements. There are shared nodes between the lower layer of skull and upper layer of CSF and lower layer of CSF and upper layer of gray matter of the brain. To represent dura matter, pia, arachnoid, meninx, falx and tentorium, shell elements are used. Connection with shared nodes is applied in whole brain of THUMS M50 version 4.1 model (Fig. 1B). The material models for different parts are available in literature [12][28-29]. In particular, a linear viscoelastic material model was used to model the response of the gray and white matter. The material of the CSF is equivalent to fluid with density equivalent to water which does not restrict the movement of brain relative to the skull.

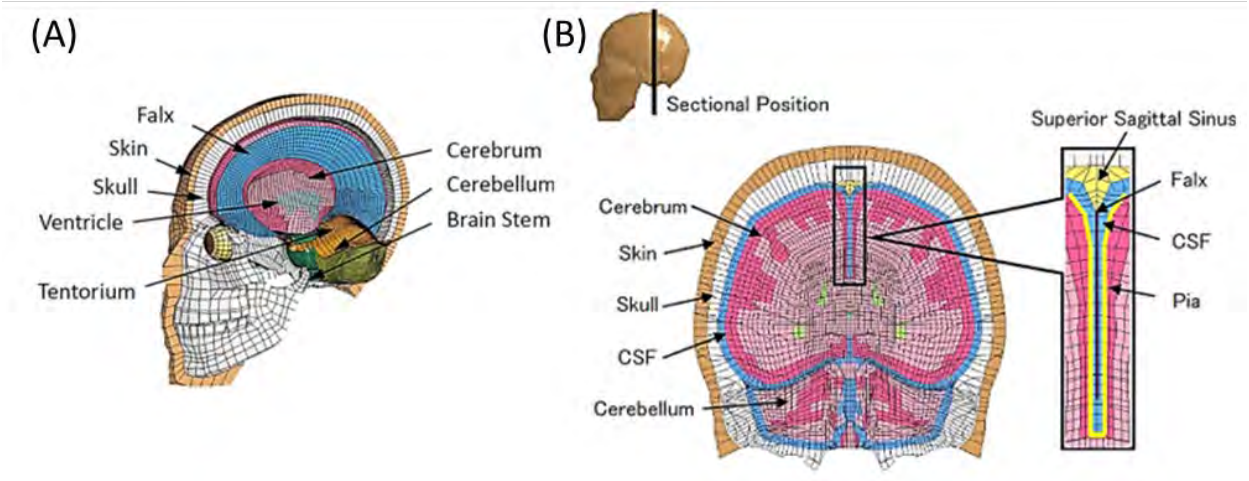

Fig. 1. Details of the original THUMS v4 FE head model: (A) sagittal view and (B) coronal view [12][29].

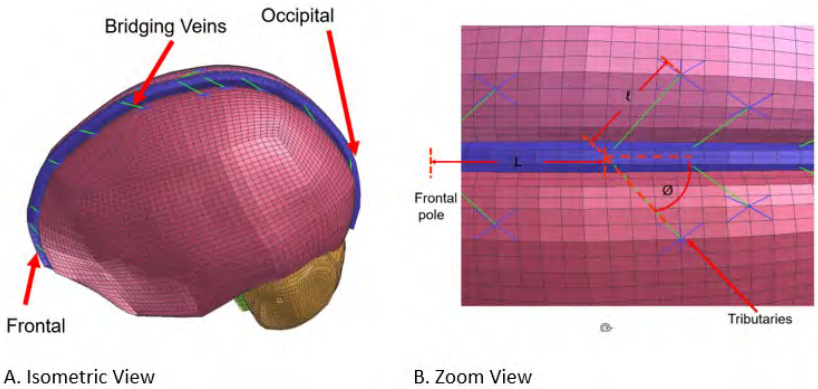

Fig. 2. Overview of FE bridging vein modelling of eTHUMSv4_HM.

Enhanced THUMS v4 head model (eTHUMSv4_HM)

The first part of the study focused on the meshing aspects of the skull and skin. To improve the skull fracture response, the single element layer of the trabecular skull and skin were re-meshed. A convergence study was conducted with meshes ranging between 2 and 8 layers of element. The reaction force, plastic strain, von Mises stress and internal energy was compared for different mesh layers obtained for simple impactor test [30]. Furthermore, element quality at temporal, occipital and sphenoid bones was improved.

In the improved version of the model, the linear viscoelastic material model for brain was replaced by hyper viscoelastic material. This is a combination of the Ogden hyper elastic material model [31] with decoupled isochoric and volumetric response and a Prony series for the viscoelastic component of the material response. The Ogden parameters were obtained by curve fitting of experimental data [32] (Fig. A4). As the white matter is 39% stiffer than gray matter and more viscous [33], in this study separate material models for gray and white matters were assigned. A second order Ogden material model was chosen for the material optimisation. The viscoelastic constants were obtained from the *in-vivo* MRI data reported by [34]. For the skull, the material models described in [12][28] were initially used and further optimised during the validation of the model to improve the skull behaviour.

To model the bridging veins, bar elements were used in VPS. One end of the bar element was connected to gray matter through One node To Multiple nodes Constraint (OTMCO). The independent nodes for the OTMCO were decided based on the tributaries for each bridging vein. The other end of the bridging vein was connected to the node of superior sagittal sinus, shared with skull node. The number of tributaries, length of bridging veins, angle between superior sagittal sinus and bridging veins, and distance from frontal pole to termination in superior sagittal sinus were obtained from [35]. Eleven pairs of bridging veins were developed (Fig. 2). Further information are provided in Table A1. A non-linear, tension-only elastic-plastic material was used for the bar element.

Experimental data for head model validation

The improved brain model was validated against pressure data from [30-36]. Nahum *et al*. [30] conducted frontal impact experiments with unembalmed PMHS. The forehead of a depressurised PMHS was impacted with a cylindrical impactor of mass 5.6 kg. The head was rotated in order to have the Frankfort anatomical plane at 45 degrees to the loading axis (Fig. 3A). The impactor velocity ranged from 4.36 m/s to 12.95 m/s. Pressure data were recorded at: the frontal lobe adjacent to the area of impact; immediately posterior and superior to the coronal and squamosal suture, respectively, in the parietal area; inferior to lambdoidal suture in the occipital bone (one in each side); and the posterior fossa in the occipital area. For test No. 37 (impactor velocity 9.94 m/s) detailed contact force (peak force=7900 N) and pressure data at different brain locations were available. At each location the pressure was extracted for multiple elements and averaged before comparing with the experimental data. The impactor material model was obtained from [8].

In the experiments of [36], unembalmed PMHS were suspended in a sitting position and impacted in the facial region by a 23.4 kg impactor at a velocity of 7 m/s in the anteroposterior direction. The pressurised PMHS heads were instrumented with a 12-accelerometer array to measure the 3D kinematics of the head. Miniature pressure transducers were placed in the subarachnoid space and in the ventricular system to measure intracranial and ventricular pressures. The linear and rotational accelerations obtained in the experiments were applied at the centre of gravity of the head model (Fig. 3B), assuming the skull to be rigid. The results from test No. MS428-2

were used for the validation of the eTHUMSv4_HM. The pressure at the frontal, occipital and lateral ventricles was extracted from the simulation for comparison with the experimental data.

To validate the relative motion between the skull and the brain, experimental data from [37-39] were used. Both [37] and [39] conducted a series of low-energy impact tests using pressurised PMHS head. Neutral density targets (NDTs) were implanted inside the PMHS brain. Their relative motion with respect to the head was tracked by high-speed bi-planar X-ray system. The head kinematics data from the experiments were implemented at the centre of gravity of the FE head (Fig. 3C). The skull was modeled rigid in order to facilitate the implementation of the 6 degree of freedom (DOF) acceleration field. The nodes situated closest to the location of NDTs in the experiments were chosen and their motion data were extracted for comparison with experimental data. The simulation results were quantified by calculating average discrepancy in minima and maxima of plots between simulation and experimental data [8][15]. Alshareef *et al*. [39] conducted a series of similar tests, where sonomicrometry was used to track the movement of piezoelectric crystals (PC) inserted in the brain. These tests targeted angular velocity of 20 rad/s and 40 rad/s, imparted independently in axial, coronal and sagittal planes with peak acceleration of 1 rad/s2, 2 rad/s2 and rad/s2 (Fig. 3D). The correlation between experiments and simulations of test subject #846 (PCs: RC9, RC15, RC16, RC18, RC20, RC23, RC28, RC29, RC31) was assessed for each available PC, displacement component (x,y,z) and loading condition for a total of 324 curve comparisons. The starting time for the comparison was moved to 10 ms to allow for the time frame where no loading was applied.

The FE skull model was validated against PMHS head-drop test data as in [40] [41]. Seventeen PMHS specimens were isolated at the level of the occipital condyles and drop tests were conducted. The PMHS head was dropped against three different surfaces with different stiffnesses and shapes. To replicate each experiment the impactor foam was modeled with crushable foam material model. The foam material parameters were obtained from [42]. The test matrix consisted of repeated tests with the same specimen, successively increasing input energies until fracture or the impact force was closer to the rated limit of the load cell. The velocity of head impact ranged from 2.44 m/s to 8.08 m/s. The eTHUMSv4_HM was aligned as described in the experiments (Fig. 3E). The velocity at contact from the experiment was then applied to the eTHUMSv4_HM. For all simulations the force-time plots were extracted and compared with the experimental response. Further, peak skull internal energy and peak force data were extracted to use as a metric to predict skull fracture.

Dynamic tensile tests were conducted on 25 bridging vein specimens, collected from six male PMHS (age 63–96 Yrs), with velocities of 5 mm/s, 20 mm/s and 50 mm/s [43]. The bridging vein specimen is fixed at one end and the other end is loaded in tensile manner. Monea *et al*. [44] conducted dynamic tests on bridging vein specimen (No: 125; female: 57 and male 68 with strain rate up to 1800 mm/s). A corridor was developed for all tests with stress-strain data and the FE model was validated for mean stress-strain data.

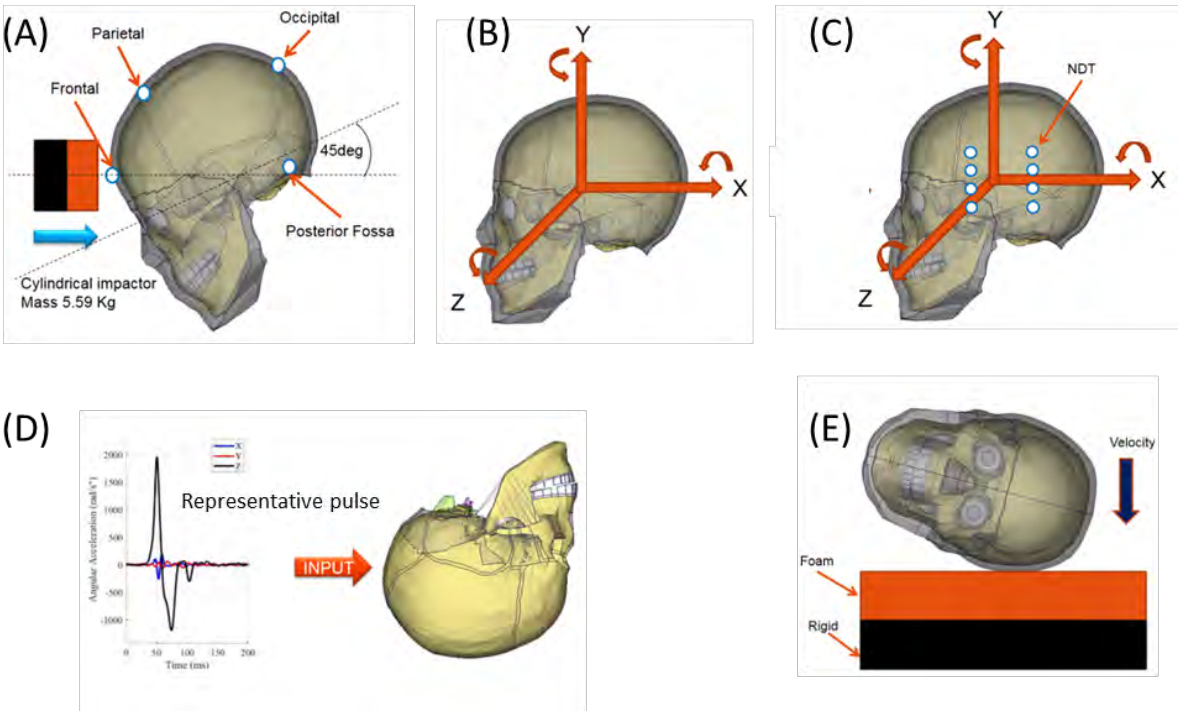

Fig. 3. Simulation setup for [30] (A), for [36] (B), for [37-38] (C), for [39] (D) and for [40-41] (E) experiments under VPS using enhanced THUMS v4 head model.

The relative deviation (percent) of peak values and the correlation value "r" (also known as sample Pearson correlation coefficient) were used to assess the model response. An r value between 0.1 and 0.3 indicates a poor correlation, while a range between 0.5 and 1 indicates a strong correlation between the curves. As the upper and lower corridors were available for skull impact experiments, the CORA (CORrelation and Analysis) score was computed to evaluate the predicted skull response.

Each setup used for the skull validation was rated independently and considered with the same weighting factor. The 40D flat, the 90D flat and the 90D cylindrical impactors were based on 6, 5 and 4 simulations (different velocity), respectively. For each of these configurations, each simulation was considered with the same weighting factor. For each of the simulations, a combination of the Corridor Method and the Correlation Method was used (CORA manual) with a weight of 0.4 and 0.6, respectively. For the Corridor Method, the inner and the outer corridors correspond to the average experimental curve plus/minus one standard deviation and plus/minus two standard deviation, respectively. For the Correlation Method, the cross-correlation function, the size and the phase shift were considered with the same weight (0.333).

Accident database and reconstruction

For the development of robust brain injury and skull fracture criteria, several real-world head trauma cases (N = 78) were collected for reconstruction. Twenty-five American football head impact events were collected from the reconstruction study by [20-21] and corrected as suggested by [45]. Twenty-nine fall cases were collected from a reconstruction study by [22], [46-47]. Ten pedestrian and vehicle occupant accident cases were collected from [48] and accident reconstructions based on Audi Accident Research Unit (AARU) accident database [49]. Fourteen volunteer sled tests conducted by the Naval Body Dynamics Lab (NBDL) were collected from the National Highway Traffic Safety Administration (NHTSA) database [50]. In all the accident cases occurrence/non-occurrence of AIS2+ brain injuries was reported. Linear and rotational acceleration at the head centre of gravity were reported for all cases except 9 fall cases from [22, 47].

Two separate methods were implemented for the fall case reconstruction. When the head accelerations data were available [46], these were implemented at the head centre of gravity. The skull was modeled rigid to facilitate the implementation of the 6 DOF acceleration field. For the 9 fall cases, the head was impacted to the respective impact surfaces at correct head orientation [47] and impact velocity [22]. For these accident simulations several mechanical parameters were extracted, such as maximum brain pressure, maximum Von Mises stress, maximum Von Mises strain, maximum principal strain (MPS), principal strain rate and combination of principal strain and strain rate (named as BIS: Brain injury Score) to derive brain injury criteria. The BIS is calculated by Eq. 1: [51]

$$BIS = 0.6 \times \epsilon + 0.4 \times \dot{\epsilon} \quad (1)$$

where ε is brain strain and $\dot{\varepsilon}$ is brain strain rate.

For the development of skull fracture criteria, 91 head trauma cases were considered. These cases consisted of experimental drop cases [40-41] in combination with a few fall accident cases [22] [47]. Different candidate parameters (maximum force, maximum skull internal energy, HIC and SFC) to predict skull fractures were extracted in each simulation.

Statistical method

To develop head injury criteria and injury risk curves, statistical analyses were carried out for all potential parameters extracted in the head trauma simulation. To find the best suitable injury predictor, receiver operating characteristic (ROC) curves were plotted. The ROC plot expresses the performance of a binary classifier system (injured vs non-injured) as its discrimination threshold is varied. The curve is generated by plotting the true positive rate (sensitivity) against the false positive rate (fall-out), which can be calculated as 1 – specificity, at various threshold settings. The area under the ROC (AUROC) curve is another measure of the test performance. The test is 100% accurate if the AUROC is 1: both the sensitivity and specificity are 1.0 (no false positives and no false negatives). On the other hand, a test that cannot discriminate between normal and abnormal corresponds to a diagonal line from (0, 0) to (1, 1) for which the AUROC is 0.5. As described in [52], AUROC values are typically between 0.5 and 1.0. Hence, the candidate parameter with the highest AUROC value results in the best injury predictor parameter. The goodness-of-fit for logistic regression models was investigated through the Hosmer–Lemeshow (HL) test. This test assesses the extent to which the observed event rates match the expected event

rates in subgroups of the model population.

The injury risk curves were generated through survival analysis of binary data assuming a log-logistic distribution (Eq. 2). Binary logistical regression was carried out using open-source statistical code R (R Project for Statistical Computing). This method involved fitting of a regression model between a number of possible injury predictors.

$$P(x) = 1 \Big/ \left(1 + \left(\frac{X}{e^{a}}\right)^{(-e^{b})}\right) \qquad (2)$$

where a and b are the location and scale parameters determined by the logistic regression. The quality of the injury risk curve was assessed in terms of average width of the 50% risk confidence interval and by normalising the x-axis of the risk curve by the input value related to 50% risk of injury.

III. RESULTS

Head Model Enhancement and validation

The convergence study showed that 4 layers of trabecular skull bone and 3 layers of skin delivered the optimum outcome. The final geometry is presented in Fig. A1. Results of the convergence study are presented in Fig. A2 for the skull and in Fig. A3 for the skin. The skull validation of the resultant contact force with respect to the experimental mean along with the experimental corridor is presented for three different impactors at the highest velocity in Fig. 6. A good agreement was found between simulations and experimental mean (average r > 0.8). The peak force differed less than 5% for all 15 load cases. The average CORA rating for the simulated 15 load cases was 0.723. The results indicates that the response predicted by the skull model correlates well with the response measured in the experiments.

The validation of the material model for the bridging vein with respect to [43-44] data is presented in Fig. 7. A good agreement was found between simulations and experimental mean (average r > 0.9).

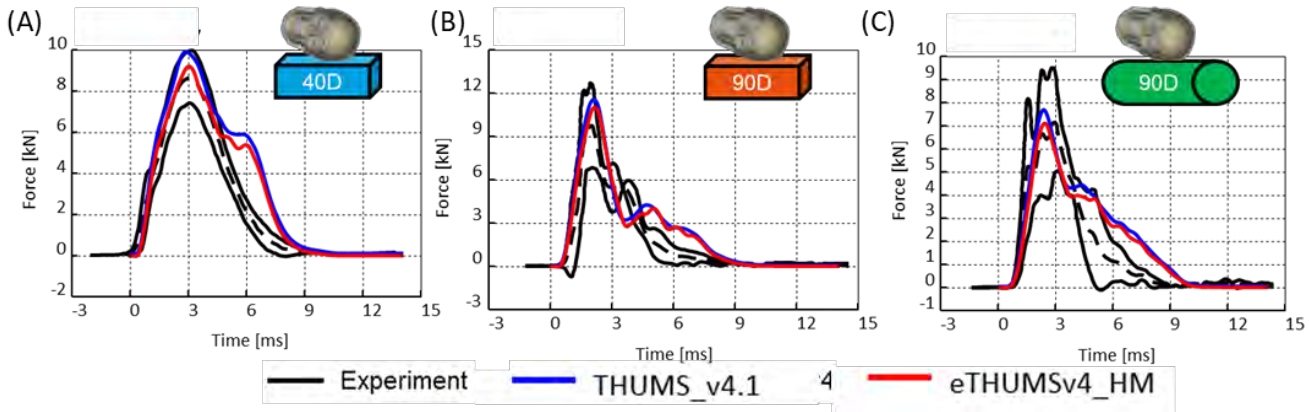

Fig. 6. Contact force comparison between simulation result (THUMS v4.1 and eTHUMSv4_HM) and experimental corridors for (A) 40D flat impactor at 6.47 m/s impact velocity, (B) 90D flat impactor at 5.46 m/s impact velocity and (C) 90D cylindrical impactor at 4.89 m/s impact velocity.

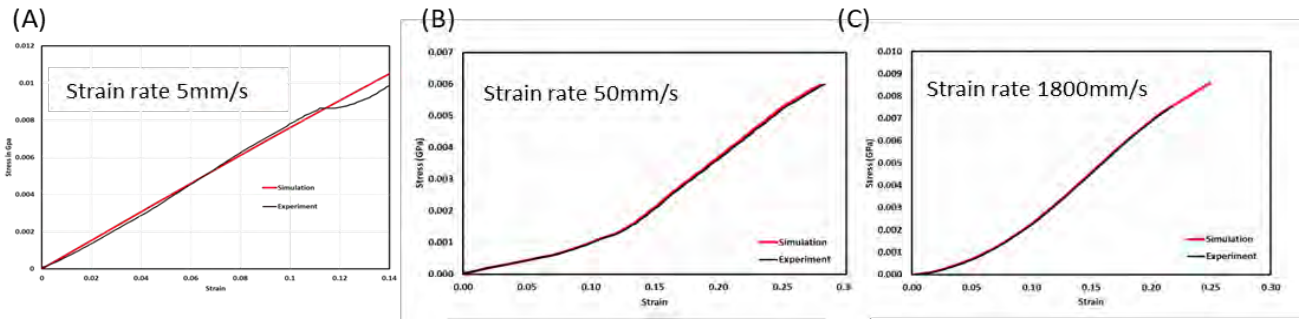

Fig. 7. Comparison of experimental and simulation data for bridging vein tests from [43] (A and B), and high strain rate tests from [44] (C).

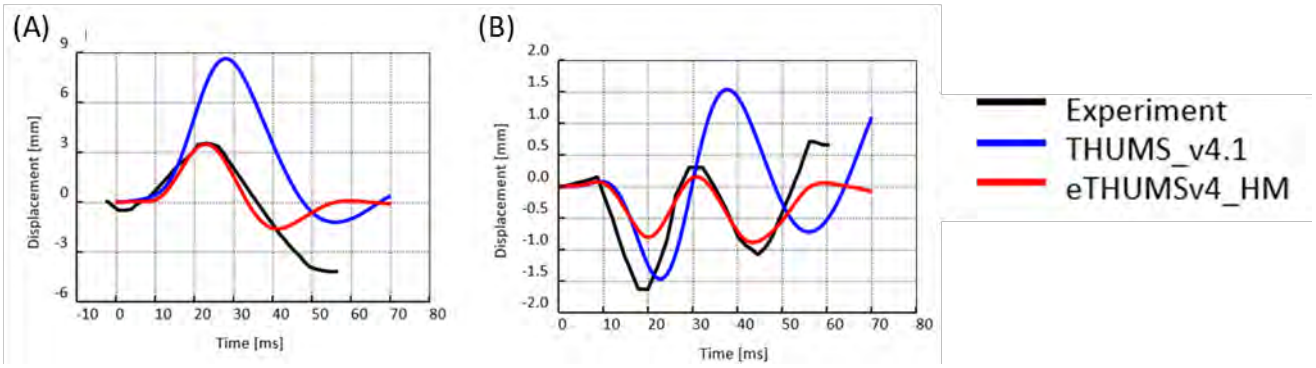

Fig. 5. Displacement time histories comparison for NDT locations in (A) X and (B) Z direction for NDT a1 for THUMS v4.1, eTHUMSv4_HM and experiment data from test C755-T2 [37-38].

The local brain kinematic response predicted by the eTHUMSv4_HM in the simulation of the experiments by [37-38] agreed with the motion measured in the tests. The results for one NDT in X and Z direction for Test C755-T2 are shown in Fig. 5. The comparison of NDT time histories between simulation and experiments is done by calculating the average discrepancy between maxima and minima. The maxima for NDT motion along X direction (for a1-NDT) deviated from the experimental maxima by less than 1%.

Table AI in the Appendix lists the correlation between the displacement (x, y, z) predicted by eTHUMSv4_HM and the displacements measured in the tests of #846 for PCs: RC9, RC15, RC16, RC18, RC20, RC23, RC28, RC29, RC31 from [39]. In general, eTHUMSv4_HM predicted well (corr. > 0.5) the motion in the sagittal plane in 61 of 102 available comparisons. Whereas in the axial plane, 34 of 96 available tests showed a correlation larger than 0.5. In the coronal plane, just 15 of 105 presented a good agreement between test and simulation.

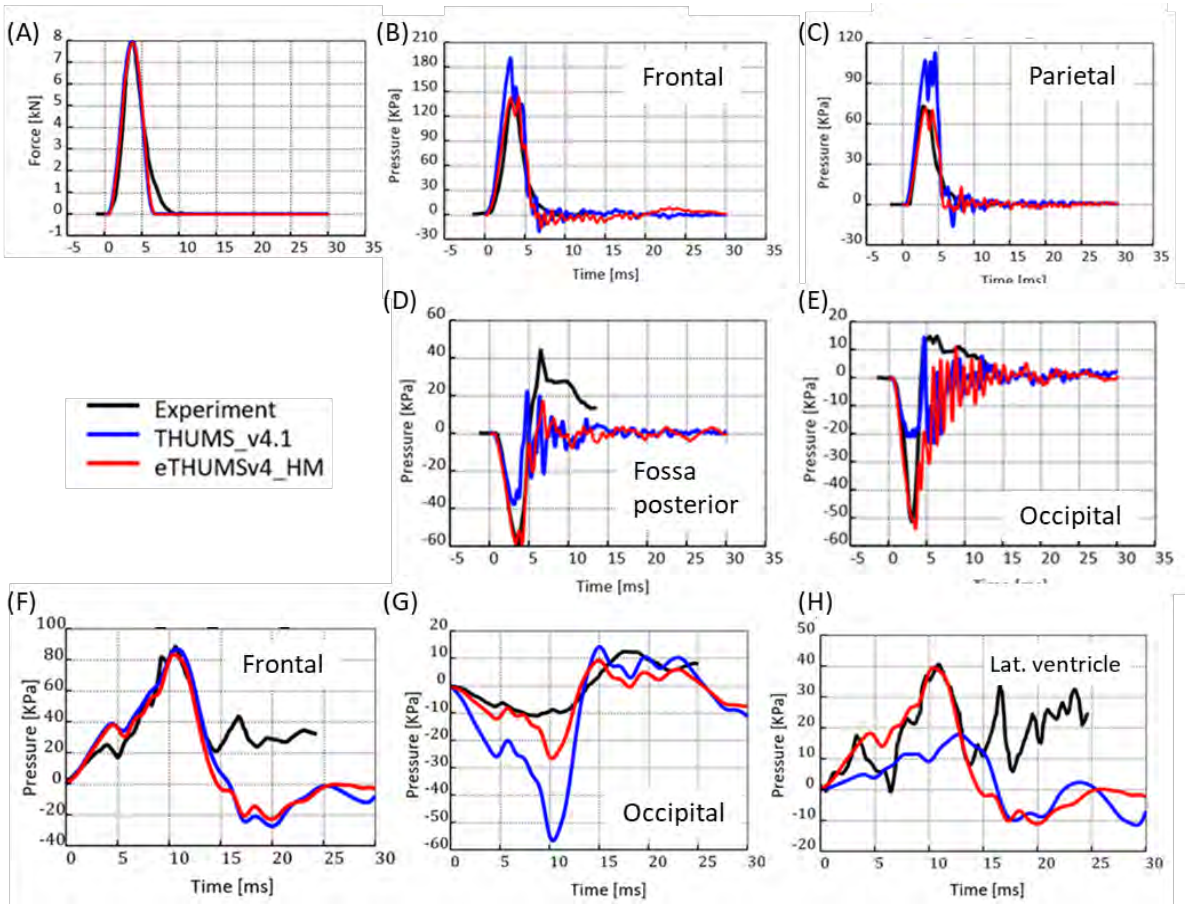

Fig. 4. Comparison of interaction force (A), frontal pressure (B), parietal pressure (C), Fossa posterior pressure (D) and occipital pressure (E) for [30]'s experiments, and comparison of frontal pressure (F), occipital pressure (G) and lateral ventricle pressure (H) for [36]'s experiments.

The simulation of [30]'s impact experiments showed a good agreement (r > 0.9) with the experimental data in terms of peak force (relative difference < 1%) and duration of impact (Fig. 4A). The intracranial pressure predicted by the eTHUMSv4_HM and the pressure measured in the experiment are reported in Fig. 4B–E. The peak pressure value was well reconstructed for all measured location (relative difference < 3%). Although the trend of the pressure response was similar at all brain locations, at the fossa posterior and occipital location the positive part of the pressure response was lower than in the experiment.

The pressure predicted by the eTHUMSv4_HM in the simulation of [36]'s experiment for Test no. MS428-2 also showed good agreement (r > 0.8). The intracranial pressure extracted at the frontal, occipital and lateral ventricle locations are reported in Fig. 4F–H. In particular, at the frontal and lateral ventricle locations the response predicted by the eTHUMSv4_HM up to 14 ms was very similar to the experiments, with a peak relative difference less than 5%.

Brain injury criterion

The above-mentioned database of head trauma was successfully reconstructed with the eTHUMSv4_HM. Different mechanical parameters, like maximum brain pressure, maximum von Mises stress, maximum von Mises strain, maximum principal strain, principal strain rate and BIS, were extracted for each simulation. The AUROC and HL p-values were computed for each parameter (Fig. 8A). The BIS presents the highest AUROC value and HL p-value of 0.99 and 0.94, respectively, among all the candidate parameters. The principal strain rate has the second highest AUROC value of 0.96 and HL p-value of 0.78. While (MPS) and von Mises show good AUROC values, the HL p-values were below 0.8. Pressure has the lowest AUROC value and HL p-value, at 0.84 and 0.58, respectively. As the BIS demonstrated the highest AUROC value and HL p-value, it was chosen to be the most suitable metric to predict the AIS2+ brain injuries. Survival analysis of binary injured and non-injured data with log-logistic distribution was conducted for different candidate parameters. Then the injury risk curve for each parameter was generated. The BIS-based injury risk presented the narrowest 50% risk confidence interval (Fig. 8B) and the steepest curve trend after normalisation (Fig. 8C) among the investigated parameters. Figure 9A shows the injury risk curve to predict brain AIS2+ injury using BIS. The white circles represent the non-injured cases and the black circles represent the cases with injury occurrence. A BIS value of 34 corresponds to a 50% risk of AIS2+ brain injury. Figure 9B shows the accident cases with (red) and without (green) injury in terms of computed BIS. The smooth transition between injured and non-injured cases indicates a good qualitative model for injury prediction as shown in Fig. A8 in appendix.

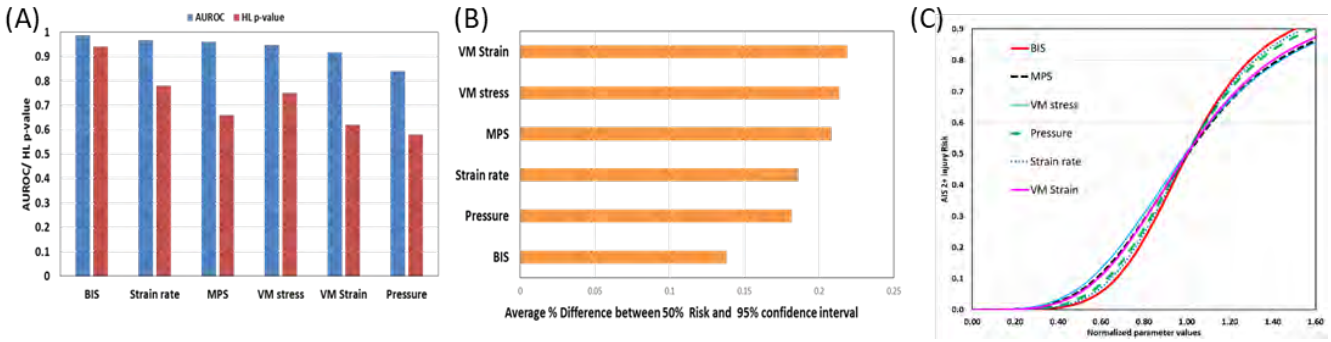

Fig. 8. Comparison of AUROC and HL p-values for different mechanical parameters (A); average width of the 50% risk confidence interval (B); comparison of 50% risk input normalised injury risk curves (C).

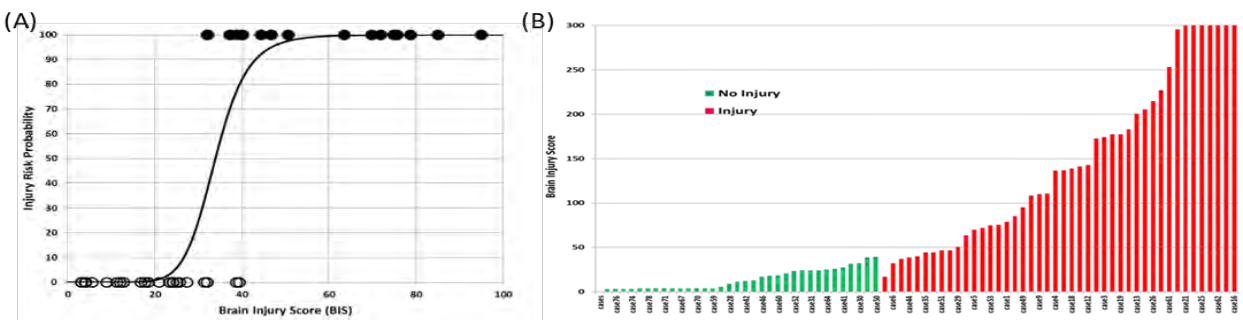

Fig. 9. Brain Injury Score (BIS) risk curve (A). BIS computed for all head injury simulation with non-injured (green) and injured (red) cases (B).

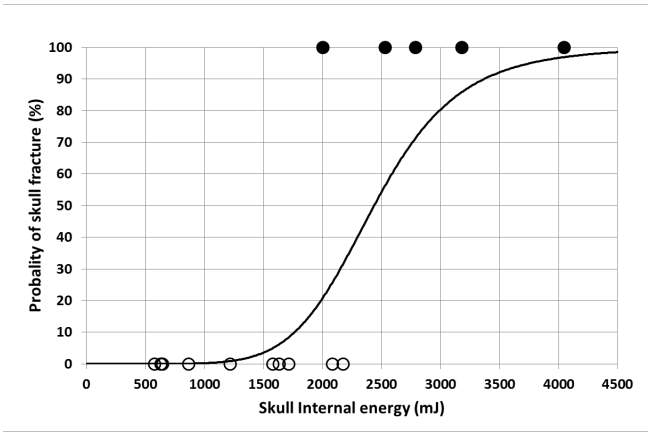

Fig. 10. Injury risk curve to predict skull fracture by using skull internal energy as injury predictor.

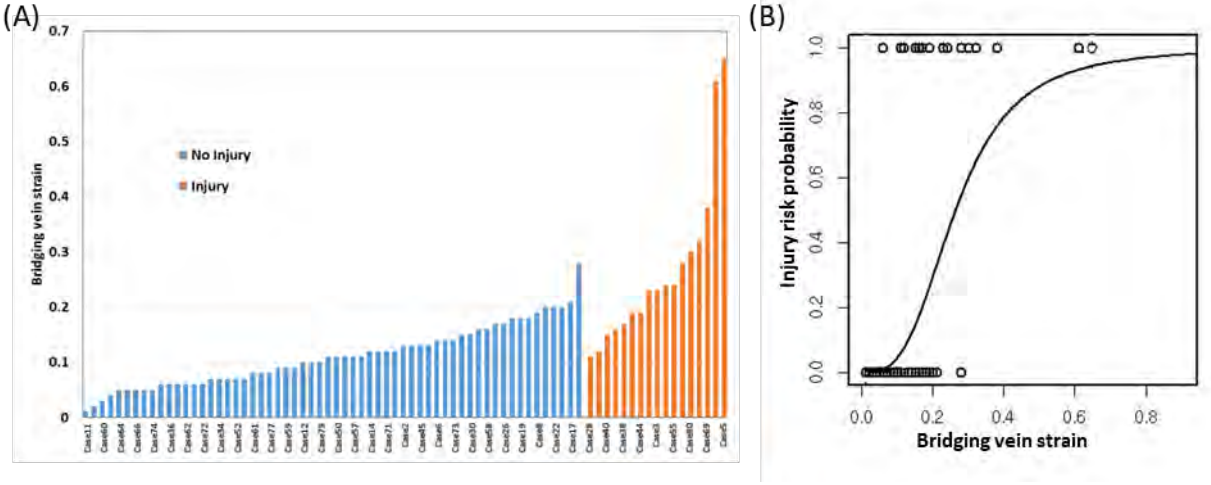

Fig. 11. Max. of all bridging veins strain computed for all head injury simulations for the non-injured (blue) cases and injured (orange) cases (A). Injury risk function of AIS3+ subdural haematoma injury (B).

Skull injury criterion

Different candidate parameters (maximum force, maximum skull internal energy, HIC and SFC) to predict skull fracture were extracted in each simulation. The AUROC for each potential parameter was computed and skull internal energy was found to have the highest AUROC value of 0.928, whereas the contact force had an AUROC value of 0.8. This indicates that skull internal energy is the most suitable metric to predict skull fracture. Further survival analysis with log-logistic distribution was done for binary skull fractured/non-fractured data for different potential parameters. The injury risk curve to predict skull fracture by considering skull internal energy as predictor is shown in Fig. 10. The white circles represent the non-fractured cases and the black circles represent the cases with skull fracture. The 50% injury risk of skull fracture was reached for a skull internal energy of 2.4 J.

Subdural haematoma criterion

A total of 80 simulations were conducted with isolated head model, including 12 rear impact tests from [53] and 68 real-world accident cases. Strain in the bridging veins (max. of all veins) was extracted and used for survival analysis. Figure 11A shows the accident cases with and without injury in terms of strain in bridging veins. The blue columns represent the non-injured cases and the orange columns represent the injured cases. The smooth transition between injured and non-injured cases indicates a good qualitative model for injury prediction. Bridging vein strain (max. of all veins) is the potential parameter and 50% risk of AIS3+ (subdural haematoma) injury is 26% strain (Fig. 11B).

IV. DISCUSSION

The objective of this study was to validate the improved head model and to develop an injury risk function to asses AIS2+ brain injury and skull fracture. The brain model was enhanced by implementing hyper viscoelastic material coming from *in vivo* [34] and *in vitro* [32] experiments.

Anisotropic material model is helpful to incorporate the effect of axon bundles for DAI prediction. Though

heterogeneity was induced in the brain model by assigning different properties to the white and gray matters of brain, use of isotropic material for the brain is a limitation of the current study. This was mainly due to a lack of compatible material model under VPS Version 2022.04. The brain behaviour was validated for pressure against experimental pressure data [30-36]. A very good agreement between the pressure predicted from the eTHUMSv4_HM and the experiment was achieved. Furthermore, the peak pressure value differed less than 5%, thus indicating a proper mechanical response of the brain. The relative motion of the brain with respect to skull was also reasonably reproduced by comparing the NDTs. The improved brain model provides qualitatively better pressure and local brain motion response than [9][12]. The material models implemented in the skull are similar to those described in [28] and were further optimised during the skull model validation to improve the system behaviour. The validation dataset included 15 head impact load cases against three surfaces having different stiffnesses and shapes. A good agreement was found between the predicted contact force and the experimental mean force with an average correlation coefficient of more than 0.8 and relative maximum force difference less than 5%. For the 15 load cases an average CORA rating of 0.723 demonstrates the robust validation of the eTHUMSv4_HM.

A total of 78 real-world accident cases were reconstructed to develop an injury criteria for the prediction of AIS2+ brain injury specific to the eTHUMSv4_HM. Several tissue-level parameters were extracted from each simulation and statistical analyses were conducted to find the best suitable predictor. BIS provided the highest correlation with the occurrence of AIS2+ brain injury among all tissue-level metrics considered in this study. In particular, the BIS provided a low TBI risk for the 14 NBDL volunteer cases where only minor TBI were reported (AIS1). The evaluation of the same volunteer cases based only on MPS indicated high risk of severe TBI (AIS2-3) [17]. This suggests that the use of strain rate in combination with MPS provides a better predictor of TBI. A further 91 head trauma cases were reconstructed using eTHUMsv4_HM in VPS platform to develop a skull fracture criteria. Skull internal energy was identified as the best parameter to predict skull fractures. This is in accordance with previous literature studies [16][26][40-54]. The 50% risk of skull fracture at 2.4 J of skull internal energy is in accordance with [16].

In the current study, most of the head trauma simulations were done by implementing head kinematics data published in the literature. The accuracy of the reconstruction is influenced by the accuracy of the published data source. Also the confidence of survival analysis is influenced by the sample size. In this study, 78 head trauma cases for head and 91 head trauma cases for skull were used to develop injury criteria. This sample size is reasonable compared to other studies in the literature [10][16]. However, higher sample size can further improve the proposed criteria. Nevertheless, the high correlation of BIS and skull internal energy with the injuries observed in the validation cases gave us confidence on the developed head model and injury risks. Furthermore, in the current study the effect of the specimen diversity (geometry and mass) was not investigated.

V. CONCLUSION

The brain and skull of the head of the existing THUMS v4 model was improved for geometry and material modeling. The improved brain model was validated for intracranial pressure behaviour and relative motion of brain with respect to skull. The skull was validated against recent drop experimental data. A good agreement was obtained during the validation of both skull and brain by comparing simulation and experimental data. In this study, 78 head trauma cases for head and 91 head trauma cases for skull were used to develop injury criteria. The internal energy was found to be the most suitable parameter to predict skull fractures. Whereas the BIS presented the highest correlation among all the candidate parameters to predict AIS2+ based brain injury. The novelty of the approach, combining both brain strain and strain rate, represents an improved method to numerically assess the risk of mild TBI in car crashes.

VI. ACKNOWLEDGEMENTS

The authors would like to acknowledge AUDI AG for funding and the Audi Accident Research Unit for providing the data for the accident reconstructions.

VII. REFERENCES

[1] Rubiano, A. M., Carney, N., Chesnut, R., Puyana, J. C. (2015) Global neurotrauma research challenges and opportunities. *Nature*, **527**: pp. S193–S197.

[2] Majdan, M., Plancikova, D., *et al*. (2016) Epidemiology of traumatic brain injuries in Europe: a cross-sectional analysis. *The Lancet Public Health*, **1**(2): e76–e83.

[3] Marin, J. R., Weaver, M. D., Mannix, R. C. (2017) Burden of USA hospital charges for traumatic brain injury. *Brain injury*, **31**(1), pp. 24–31.

[4] Brazinova, A., Rehorcikova, V., *et al*. (2016) Epidemiology of Traumatic Brain Injury in Europe: A Living Systematic Review. *Journal of Neurotrauma*, **33**: pp. 1–30.

[5] Faul, M. D., Wald, M. M., Xu, L., Coronado, V. G. (2010) Traumatic brain injury in the United States; Emergency Department Visits, Hospitalizations, and Deaths, 2002–2006. Centers for Disease Control and Prevention. Atlanta, GA.

[6] Abbreviated injury scale, update 2008, Copyright, 2008, Association for the Advancement of Automotive Medicine, Barrington, IL, USA.

[7] Takhounts, E. G., Hasija, V., *et al*.. (2008) Investigation of traumatic brain injuries using the next generation of simulated injury monitor (SIMon)finite element head model. *Stapp Car Crash Journal*, **52**: pp. 1–32.

[8] Sahoo, D., Deck, C., Willinger, R. (2016) Brain injury tolerance limit based on computation of axonal strain. *Accident Analysis and Prevention,* **92**: pp. 53–70.

[9] Mao, H., Zhang, L., *et al*. (2013) Development of a finite element human head model partially validated with thirty-five experimental cases. *Journal of Biomechanical Engineering*, 135(11): pp. 111002–111015.

[10] Giordano, C., Kleiven, S. (2014) Evaluation of axonal strain as a predictor for mild traumatic brain injuries using finite element modeling. *Stapp Car Crash Journal*, **58**: pp. 29–62.

[11] Ji, S., Zhao, W., *et al*. (2014) Group-wise evaluation and comparison of white matter fiber strain and maximum principal strain in sports-related concussion. *Journal of Neurotrauma,* 7: pp. 441-454.

[12] Atsumi, N., Nakahira, Y., Iwamoto, M. (2016) Development and validation of a head/brain FE model and investigation of influential factors on the brain response during head impact. *International Journal of Vehicle Safety*, **9**.

[13] Ji, S., Ghadyani, H., *et al.* (2014) Parametric comparisons of intracranial mechanical responses from three validated finite element models of the human head. *Annals of Biomedical Engineering,* **42**(1): pp. 11–24.

[14] Yang K. H. Basic Finite Element Method as Applied to Injury Biomechanics, *Academic Press.*1st Edition, Paperback ISBN: 9780128098318, London, UK, 2017.

[15] Kleiven, S. (2007) Predictors for traumatic brain injuries evaluated through accident reconstruction. *Proceedings of the 51st Stapp Car Crash Conference*, SAE, 2007, San Diego, California.

[16] Deck, C., Willinger, R. (2008) Improved head injury criteria based on head FE model. *International Journal of Crashworthiness,* **13**(6): pp. 667–678.

[17] Sanchez, E. J., et al. (2017) Evaluation of head and brain injury risk functions using sub injurious human volunteer data. *Journal of Neurotrauma*, 34: pp. 2410–24.

[18] German In-depth Accident Study. https://www.gidas.org

[19] Audi Accident Research Unit accident database. Internet: https://www.aaru.de/aaru/ablaufdiagramm/

[20] Newman, J., Beusenberg, M., *et al*. (1999) A new biomechanical assessment of mild traumatic brain injury—Part1—methodology. *Proceedings of the IRCOBI Conference*, 1999, Sitges, Spain.

[21] Newman, J., Barr, C., *et al*. (2000) A new biomechanical assessment of mild traumatic brain injury—part 2—results and conclusions. *Proceedings of the IRCOBI Conference*, 2000, Montpellier, France.

[22] Post, A., Taylor, A., *et al*. (2017) A biomechanical analysis of traumatic brain injury for slips and falls from height. *Trauma*, doi.org/10.1177/1460408617721564.

[23] Rashid, B., Destrade, M., Gilchrist, M. D. (2012) Mechanical characterization of brain tissue in compression at dynamic strain rates. *Journal of the Mechanical Behavior of Biomedical Materials*, **10**: pp. 23–38.

[24] McElhaney, J. H., Roberts, V. L., Hilyard, J. F. (1976) Properties of human tissues and components: nervous tissues, in Handbook of human tolerance, p. 143. *Automobile Research Institute Inc.*, Tokyo, Japan.

[25] Arfanakis, K., Haughton, V. M., *et al.* (2002) Diffusion tensor MR imaging in diffuse axonal injury. *American Journal of Neuroradiology,* **23**: pp. 794–802.

[26] Sahoo, D., Deck, C., Yoganandan, N., Willinger, R. (2016) Development of skull fracture criterion based on real-

world head trauma simulations using finite element head model. *Journal of the Mechanical Behavior of Biomedical Materials,* **57**: pp. 24–41.

[27] King, A. I., Yang, K. H., Zhang, L., Hardy, W. N., Viano, D. C. (2003) Is head injury caused by linear or angular acceleration? *Proceedings of the IRCOBI Conference*, 2003, Lisbon, Portugal.

[28]Kimpara, H., Nakahira, Y., *et al*. (2006) Investigation of anteroposterior head-neck responses during severe frontal impacts using a brain-spinal cord complex FE model. *Stapp Car Crash Journal,* **50**: pp. 509–544.

[29] Iwamoto, M., Atsumi, N., Nakahira, Y., Hirabayashi, S. (2016) Development of Human Head/Brain FE Model with Material Modeling of Brain Parenchyma and Its Application to Investigation on Head Rotational Injury Mechanism. *6th International Symposium: Human Modeling and Simulation in Automotive Engineering*, 2016, Heidelberg, Germany.

[30]Nahum, A., Smith, R., Ward, C. (1977) Intracranial pressure dynamics during head impact. *Proceedings of the 21st Stapp Car Crash Conference*, 1977, Warrendale, PA.

[31]Holzapfel, G. A. Nonlinear Solid Mechanics. A Continuum Approach for Engineering. *Wiley, Chichester*, England, UK, 2000.

[32] Franceschini, G. (2006) The mechanics of human brain tissue. PhD thesis, University of Trento, Italy.

[33] Budday, S., Nay, R., *et al*. (2015) Mechanical properties of gray and white matter brain tissue by indentation. *Journal of the Mechanical Behavior of Biomedical Materials*, **46**: pp: 318–30.

[34] Kruse, S. A., Rose, G. H., *et al*. (2007) Magnetic resonance elasto-graphy of the brain. *NeuroImage,* **39**: pp. 231–237.

[35]Oka, K., Rhoton Jr, A. L., Barry, M., Rodriguez, R. (1985) Microsurgical anatomy of the superficial veins of the cerebrum. *Neurosurgery*, **17**(5): pp. 711–748.

[36]Trosseille, X., Tarriere, C., Lavaste, F., Guillon, F., Domont, A. (1992) Development of a F.E.M. of the human head according to a specific test protocol. *Proceedings of the 36th Stapp Car Crash Conference*, 1992, Seattle, Washington, USA.

[37]Hardy, W. N., Foster, C. D., *et al*. (2001) Investigation of head injury mechanisms using neutral density technology and high-speed biplanar X-ray. *Stapp Car Crash Journal,* **45**: pp. 337–368.

[38] Hardy, W. N., Mason, M. J., *et al*. (2007) A study of the response of the human cadaver head to impact. *Stapp Car Crash Journal,* **51**: pp. 17–80.

[39] Alshareef, A., Giudice, J. S., Forman, J., Salzar, R. S., Panzer, M. B. (2018) A novel method for quantifying human in situ whole brain deformation under rotational loading using sonomicrometry. *Journal of Neurotrauma*, **35**(5): pp. 780–789.

[40]Sahoo, D., Deck, C., Yoganandan, N., Willinger, R. (2013) Anisotropic composite human skull model and skull fracture validation against temporo-parietal skull fracture. *Journal of the Mechanical Behavior of Biomedical Materials,* **28**: pp. 340–353.

[41]Yoganandan N, Pintar FA. Biomechanics of temporo-parietal fracture. Clin. Biomech, 2004, 19:225–239.

[42]Sahoo D, Deck C, Yoganandan N, Willinger R. Development of skull fracture criterion based on real-world head trauma simulations using finite element head model. JMBBM. 2016, 57:24-41.

[43]Delye, H., Verschueren, P., *et al*. (2006) Biomechanical Properties of Superier Sagittal Sinus-Bridging Vein Complex. *Stapp Car Crash Journal,* **50**: pp. 625–636.

[44] Monea, A. G., Baeck, K., *et al*. (2014) The biomechanical behaviour of the bridging vein–superior sagittal sinus complex with implications for the mechanopathology of acute subdural haematoma. *Journal of the Mechanical Behavior of Biomedical Materials*, **32**: pp. 155–165.

[45] Sanchez, E. J., Gabler, L.F., *et al*. (2018) A re-analysis of football impact reconstructions for head kinematics and finite element modeling. *Clinical Biomechanics,* doi.org/10.1016/j.clinbiomech.2018.02.019.

[46]Post, A. (2013). The influence of dynamic response characteristics on traumatic brain injury. Dissertation, University of Ottawa (Canada).

[47]Post, A., et al. (2018). Falls resulting in mild traumatic brain injury and focal traumatic brain injury: a biomechanical analysis. *International journal of crashworthiness*, 23(3), 278-289.

[48]Franklyn, M., Fildes, B., Zhang, L., Yang, K., Sparke, L. (2005) Analysis of finite element models for head injury investigation: reconstruction of four real-world impacts (No. 2005-22-0001). *SAE Technical Paper*.

[49] Coulongeat, F., Roth, F., Schenk, T., Seibert, D. (2014) Simulation of a real accident with a pedestrian using a FE human model: potential from the view of Integrated Safety. *Proceedings of the IRCOBI Conference*, 2014,

Berlin, Germany.
[50]NHTSA, Biomechanics Test Database on select test parameters. Internet: https://www-nrd.nhtsa.dot.gov/database/VSR/bio/QueryTest.aspx.
[51]Sahoo D, Coulongeat F, Fuerst F, Marini G, Comparison of Head Injury criteria Based on Real-World Accident Simulations under Visual Performance Solution (VPS), *Proceedings of the IRCOBI Conference*, 2020, Munich, Germany.
[52] Metz, C. E. (1986) ROC methodology in radiologic imaging. *Investigative Radiology,* **21**: pp. 720–733.
[53] Depreitere, B., Van Lierde, C., *et al.* (2006) Mechanics of acute subdural hematomas resulting from bridging vein rupture. *Journal of Neurosurgery*, **104**(6): pp. 950–956.
[54]Delye, H., Verschueren, P., *et al*. (2007) Biomechanics of frontal skull fracture. *Journal of Neurotrauma,* **24**(10): pp. 1576–1586.

VIII. APPENDIX

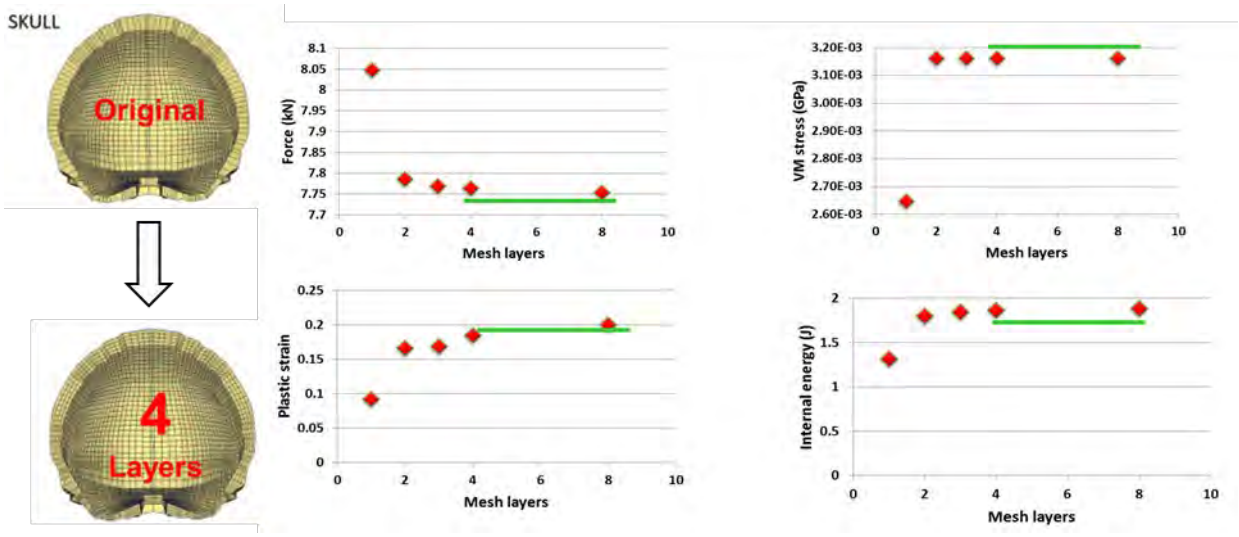

Fig. A1. Convergence study for the skull of eTHUMSv4_HM

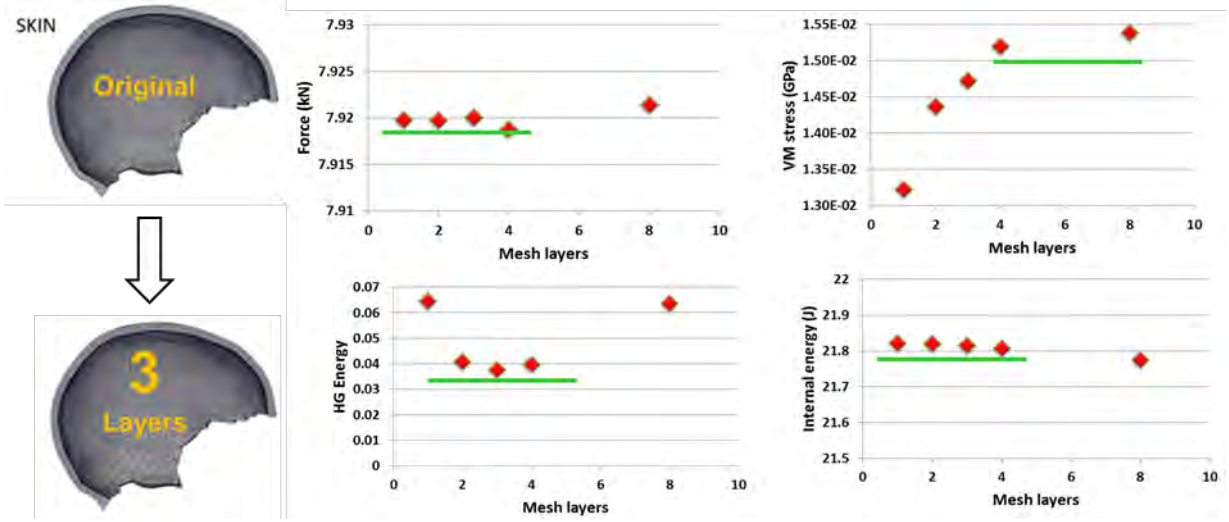

Fig. A2. Convergence study for the skin of eTHUMSv4_HM

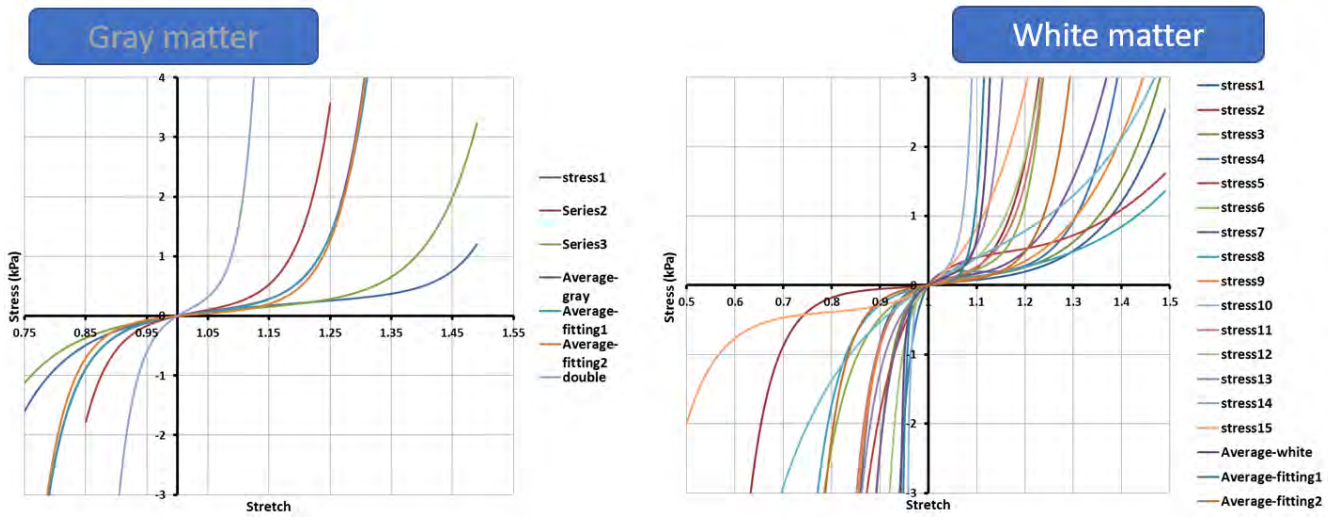

Fig. A4. Material properties for gray and white matter from [32]

TABLE AI

LENGTH, DIAMETER, NUMBER OF TRIBUTARIES, ANGLE BETWEEN SUPERIOR SAGITTAL SINUS AND BRIDGING VEINS USED IN THE ENHANCED THUMSV4.1 HEAD MODEL [35]

Bridging veins	Size (mm) Range (Average)		Number of Tributaries Range (Average)		Angle between superior sagittal and veins (in Degree) Range (Average)	
	Oka etal. 1985	Current study	Oka etal. 1985	Current study	Oka etal. 1985	Current study
Frontopolar	1.1-2.6 (2.3)	2.3	2-6 (3.1)	3	85-150 (110)	110
Anterior frontal	1.2-2.7 (2.2)	2.2	2-6(3.4)	4	55-155 (110)	110
Middle frontal	1.5-5.3 (2.7)	2.7	2-6 (3.5)	4	20-160 (85)	85
Posterior frontal	0.8-3.4 (2.3)	2.3	2-7 (4.3)	5	15-105 (65)	65
Precentral	1.8-8.0 (2.8)	2.8	2-7 (3.8)	4	20-80 (50)	50
Central	1.8-4.0 (2.5)	2.5	2-6 (3.7)	4	10-95 (45)	45
Vein of Trolard	2.0-5.0 (3.3)	3.3	4-7 (5.4)	6	20-95 (50)	50
Post central	2.3-4.0 (2.9)	2.9	2-7 (3.6)	4	15-90 (40)	40
Anterior parietal	1.2-4.0 (2.2)	2.2	2-5 (3.5)	4	0-55 (25)	25
Posterior parietal	0.9-4.0 (2.5)	2.5	2-6 (3.7)	4	0-32 (15)	15
Occipital	1.7-3.8 (2.0)	2.0	3-8 (4.1)	4	0-45 (10)	15

TABLE A2

CORRELATION VALUES BETWEEN THE DISPLACEMENT (X, Y, Z) PREDICTED FROM ETHUMSV4_HM AND THE DISPLACEMENTS MEASURED IN THE TESTS OF #846 FOR PCS: RC9, RC15, RC16, RC18, RC20, RC23, RC28, RC29, RC31 [39]

Receiver			RC9	RC15	RC16	RC18	RC20	RC23	RC28	RC29	RC31
Axial	20w_30ms	X	0,56	0,18	0,43	-	0,82	0,16	0,19	0,35	0,31
		Y	0,32	0,31	0,06	-	0,72	0,63	0,54	0,33	0,39
		Z	-0,23	0,06	0,05	-	-0,76	0,27	0,45	0,77	-0,10
	20w_60ms	X	0,55	0,48	0,64	0,54	0,66	-0,36	0,18	0,01	0,52
		Y	-0,18	0,55	-0,22	0,46	0,73	0,63	0,65	0,35	0,46
		Z	-0,18	0,02	-0,32	-0,13	-0,70	0,56	0,59	0,66	-0,22
	40w_30ms	X	0,47	0,11	0,54	0,33	-	-0,29	-	0,82	0,17
		Y	-0,03	0,25	0,25	0,04	-	0,63	-	0,42	0,25
		Z	-0,02	-0,06	-0,03	0,31	-	0,86	-	-0,02	0,19
	40w_60ms	X	0,60	0,57	0,73	0,53	0,59	-	0,07	0,46	0,57
		Y	-0,28	0,61	-0,32	0,43	0,71	-	0,77	0,41	0,59
		Z	-0,27	0,56	-0,62	0,52	-0,83	-	0,34	-0,09	-0,24
Coronal	20w_30ms	X	-0,06	0,09	-	-0,47	-0,11	-0,02	0,21	0,36	-0,54
		Y	0,31	0,26	-	0,02	-0,06	0,42	0,33	0,43	-0,23
		Z	0,31	0,32	-	0,28	0,53	0,39	-0,63	0,21	0,33
	20w_60ms	X	-0,35	0,50	-0,08	-0,45	0,40	-0,09	0,23	0,41	-0,46
		Y	0,41	0,30	0,37	0,11	0,42	0,17	0,34	0,57	-0,11
		Z	0,45	0,34	0,59	0,48	0,64	0,57	-0,03	0,27	0,45
	40w_30ms	X	-0,50	0,12	0,14	-0,21	0,13	0,30	0,18	0,41	-0,34
		Y	0,26	0,13	0,20	0,22	-0,20	0,47	0,24	0,58	0,30
		Z	0,28	0,11	0,44	0,29	0,48	0,49	0,21	0,34	0,27
	40w_60ms	X	0,16	0,28	0,08	-0,07	0,10	0,42	0,43	-0,09	0,09
		Y	0,51	0,40	0,48	0,07	0,45	0,27	0,49	0,69	-0,06
		Z	0,55	0,40	0,70	0,59	0,68	0,51	0,04	0,37	0,59
Sagittal	20w_30ms	X	0,71	0,77	0,78	0,58	0,80	0,26	0,79	0,86	0,56
		Y	0,07	0,21	-0,02	0,21	0,51	-0,56	0,33	-0,01	0,22
		Z	-0,36	0,76	-0,56	0,61	0,90	-0,56	0,67	0,38	0,71
	20w_60ms	X	0,75	0,70	0,66	0,52	0,52	0,18	0,80	0,87	0,57
		Y	-0,10	0,06	-0,03	0,46	0,13	-0,09	0,18	-0,01	0,23
		Z	-0,20	0,70	-0,46	0,66	0,83	-0,43	0,72	0,61	0,64
	40w_30ms	X	0,86	0,89	-	0,77	0,87	-	0,93	0,92	0,80
		Y	0,55	0,69	-	0,81	0,45	-	0,73	0,12	0,40
		Z	-0,85	0,84	-	0,78	0,93	-	0,82	0,50	0,80
	40w_60ms	X	0,82	0,81	0,78	0,81	0,68	0,79	0,84	0,80	0,37
		Y	0,28	0,14	0,27	0,30	0,64	-0,40	0,65	0,31	0,08
		Z	-0,25	0,79	-0,50	0,79	0,81	-0,70	0,76	0,51	0,77

Legend:
- Loading axis
- 0,35 < corr. < 0,5
- corr. > 0,5

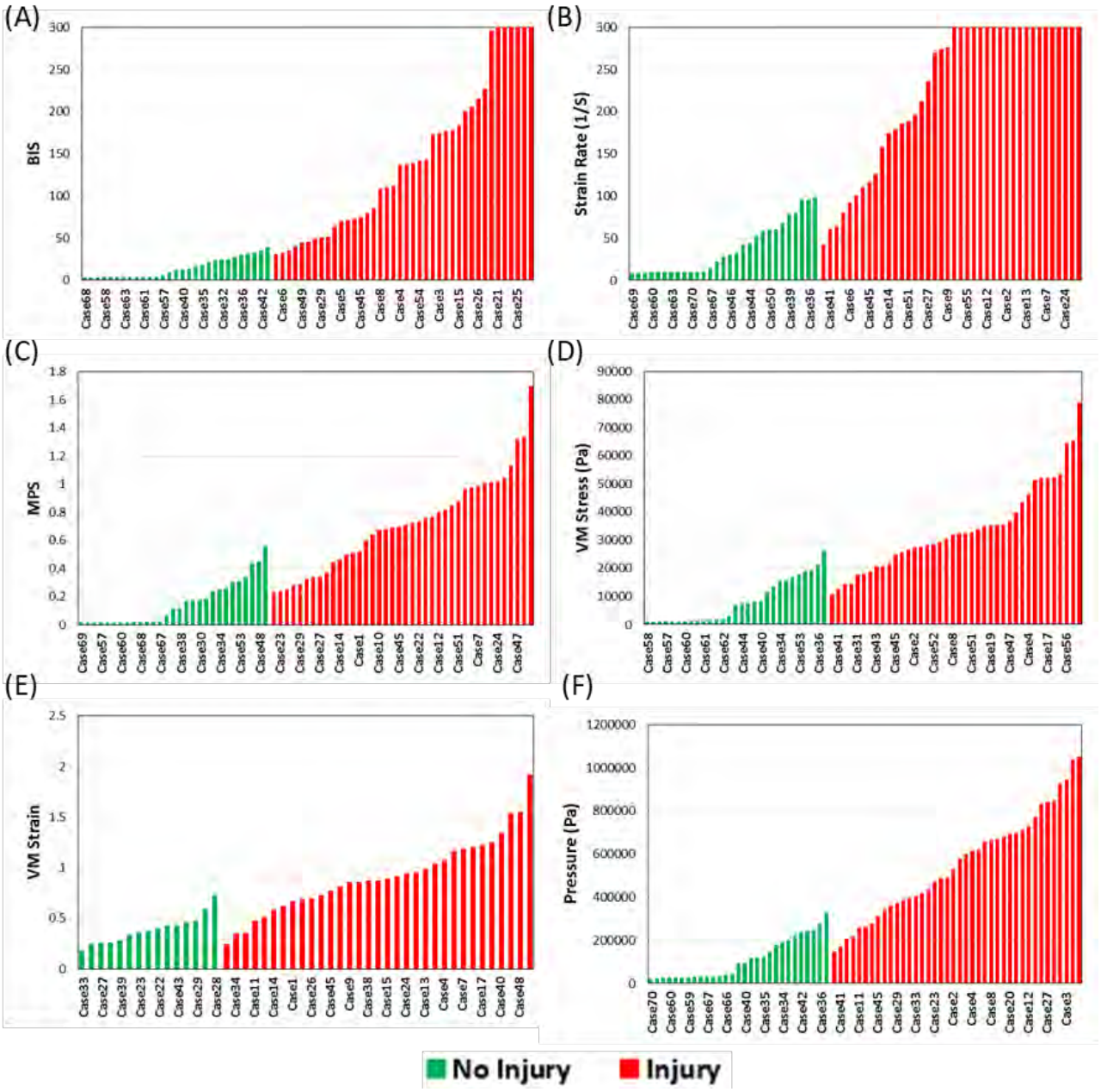

Fig. A8. (A) Brain Injury Score BIS, (B) strain rate, (C) MPS, (D) von Mises stress, (E) von Mises strain, (F) Pressure computed for all head injury simulation and displayed the non-injured cases (green) and injured cases (red).